DNA Translocation in Nanometer Thick Silicon Nanopores

Supporting Information

Julio A. Rodríguez-Manzo[†] *Matthew Puster,*[†,‡] *Adrien Nicolaï,*[§] *Vincent Meunier,*[§,‖] *and Marija Drndić*[†]

† Department of Physics and Astronomy, University of Pennsylvania, Philadelphia, Pennsylvania 19104, United States.

‡ Department of Materials Science and Engineering, University of Pennsylvania, Philadelphia, Pennsylvania 19104, United States.

§ Department of Physics, Applied Physics and Astronomy, Rensselaer Polytechnic Institute, Troy, New York, 12180, United States.

‖ Department of Materials Science and Engineering, Rensselaer Polytechnic Institute, Troy, New York, 12180, United States.

Table of contents

SI-1: Effective thickness calculation

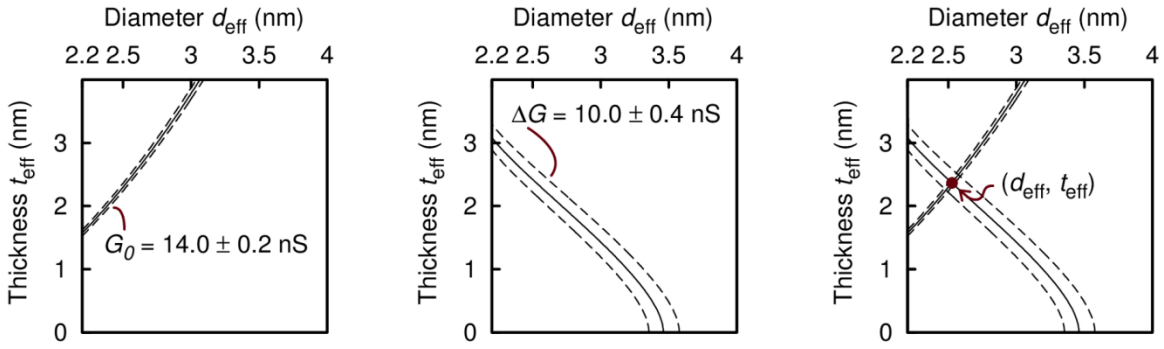

For cylindrical nanopores, the G_0 and ΔG dependence on nanopore diameter d and membrane thickness t has been modeled as:[1]

$$G_0 = \sigma\left(\frac{4\,t}{\pi\,d^2} + \frac{1}{d}\right)^{-1} \qquad (1)$$

$$\Delta G = \sigma\left(\frac{4\,t}{\pi\,d^2} + \frac{1}{d}\right)^{-1} - \sigma\left(\frac{4\,t}{\pi\left(d^2 - {d_{DNA}}^2\right)} + \frac{1}{\sqrt{d^2 - {d_{DNA}}^2}}\right)^{-1} \qquad (2)$$

where σ is the electrolyte conductivity and d_{DNA} is the DNA diameter, considered to be 2.2 nm for dsDNA. The experimentally obtained values of G_0 and ΔG are substituted into these expressions, where constant values of G_0 or ΔG can be thought of as isolines in a diameter-thickness space. The crossing of two such isolines (*i.e.*, the set of d and t that satisfy both equations) defines what we refer to as the nanopore effective diameter and thickness (d_{eff}, t_{eff}). The above Figure illustrates an example of this procedure for experimental values of G_0 = 14.0 ± 0.2 and ΔG = 10.0 ± 0.4. The left and center panels show isolines corresponding to G_0 and ΔG, respectively. Dashed lines indicate the estimated errors. The right panel shows the crossing of the two isolines, indicated by a dot. For this case (d_{eff}, t_{eff}) = (2.5 nm, 2.3 nm). We are aware that

other analytical and numerical models have been proposed in the literature,[2–4] but the differences become less significant in the limit of small diameters and thicknesses.

SI-2: Ionic current trace showing translocations of 400 bp dsDNA at 500 mV

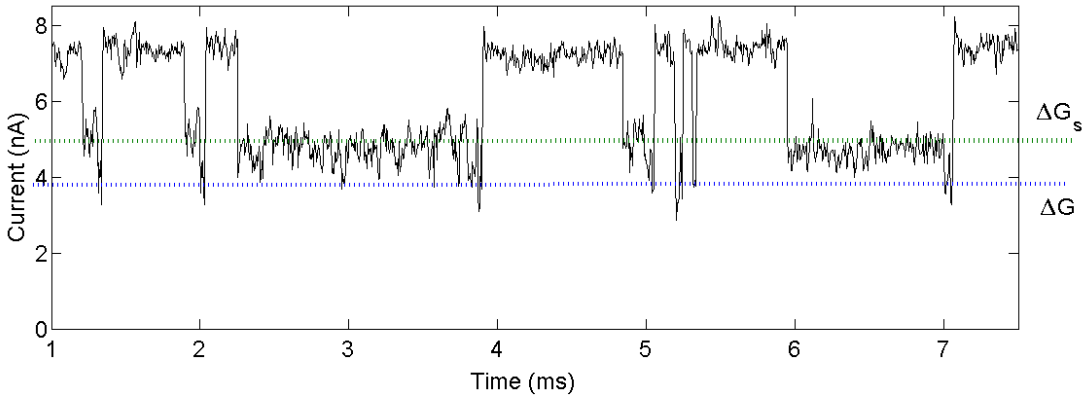

The two-level translocation structure (shallow level ΔG_s and deep level ΔG, where $\Delta G = \Delta I / V$) was also observed for 400 bp dsDNA, although with less definition when compared with the longer 15 kbp dsDNA fragments. There are two general event timescales, both of which are shown here: 1) long-time events with a noisy shallow level and a short deep level and 2) short-time events with very distinct two levels. Since the 400 bp dsDNA fragments are almost 40 times shorter that the 15kbp dsDNA fragments, it is reasonable that the ΔG level indicating translocation is very short and close to our time-resolution limit.

SI-3: Analysis of electrolyte conductivity

The following is the procedure for obtaining the electrolyte conductivity σ for various temperatures and salt concentrations for results listed in Table 1 from the literature when σ was not directly measured. Data values were obtained from the CRC Handbook of Chemistry and

Physics (HCP).[5] At 20°C, the conductivity is given directly as a function of mass % in the table titled "electrical conductivity of aqueous solutions". Conversions between mass %, molality, and molarity at 20°C are given in the table titled "concentrative properties of aqueous solutions: density, refractive index, freezing point depression, and viscosity". The HCP also provides information about σ as a function of temperature in 5°C increments for 0.01, 0.1 and 1 m KCl (table titled "standard KCl solutions for calibrating conductivity cells"). Assuming a linear dependence of σ between 0.1 and 1 m KCl and also a linear dependence of σ between 5°C increments, allows for an approximation of σ for a wide range of temperature and concentration. Similar procedures were used for LiCl and NaCl, except the conductivity cell calibration data is not given and the relationship between concentration and σ becomes non-linear for high concentrations. A non-linear fit for σ vs. mass % can be obtained, and again we assume a linear relationship between temperature and σ for small variations away from 20°C.

SI-4: Statistical analysis of translocations data

Translocation events measured at 500 mV were selected and recorded when they fit the following criteria: *i*) maximum translocation time duration = 50 ms, *ii*) minimum translocation time duration = 20 μs, and *iii*) change from ionic current baseline > 1 nA, where the baseline was calculated as the mean current about the translocation. A quick view of the data is provided by the single-point-per-event scatter plot and its histogram, using the lowest point in each translocation, as shown below for a typical example:

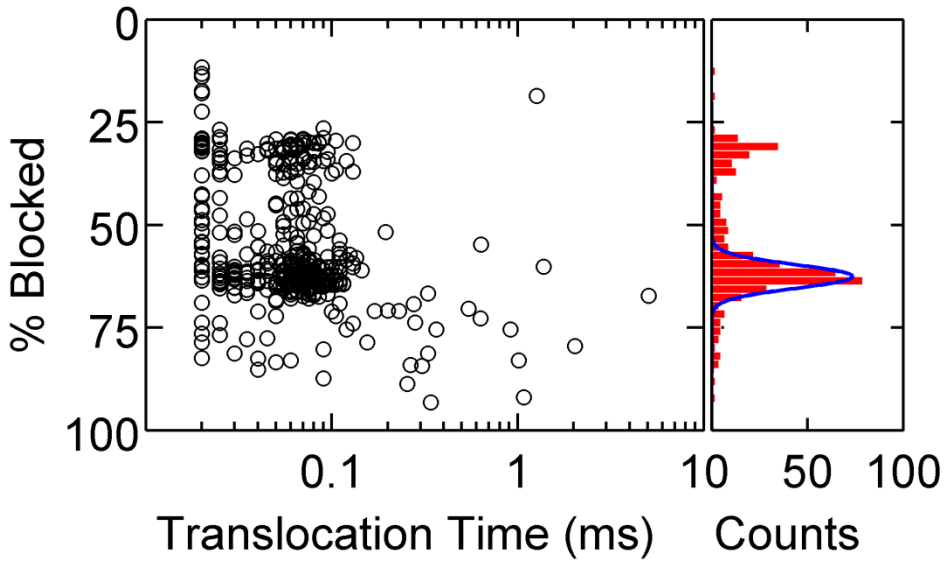

Here, the recorded translocation times are unaffected by the choice of the lowest point within each translocation, but the most likely % blocked value (ΔG / G_0 × 100) shows the maximum % blocked, rather than an average of the noise, because it uses the lowest point in each event. A more accurate picture in terms of % blocked is achieved by looking at the all-points-per-event histograms, in which we plot every point from 3 × (translocation time), such that the baseline current contributes points at 0 % blocked. An example is given below. Translocation times filter: 15 μs to 50 ms.

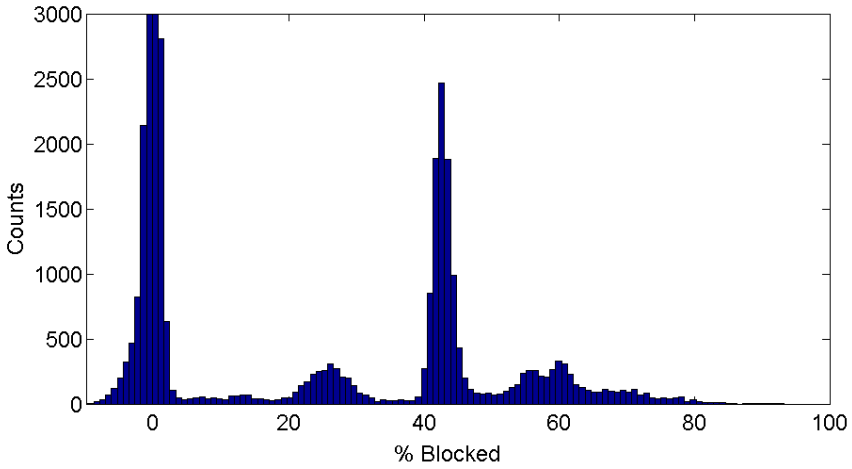

The presence of many peaks in the all-points-per-event histogram is a common occurrence, in contrast to the single-point-per-event histogram, which shows two clearly defined peaks that unambiguously represent the deep translocation level (ΔG) and the shallow level (ΔG_s). From the single-point-per-event scatter plot we determine the important time range in which events occur, and as the data is filtered in time in the all-points histograms to only the events occurring within that range, the two main peaks begin to be resolved. The largest peak at 0 % blocked represents the points associated with the baseline current. The additional peaks found in the histogram above come from a small number of events, which occur for times much longer than the average translocation time. Translocation time filter: (top) 20 μs to 2 ms and (bottom) 20 μs to 0.2 ms.

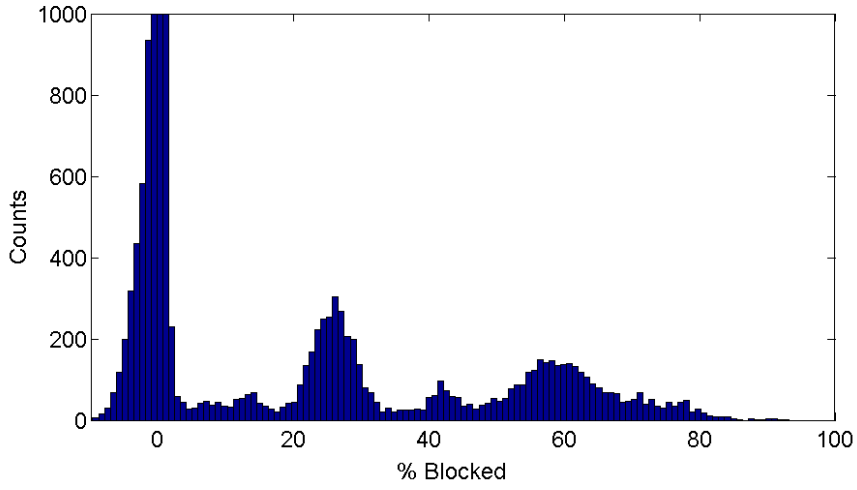

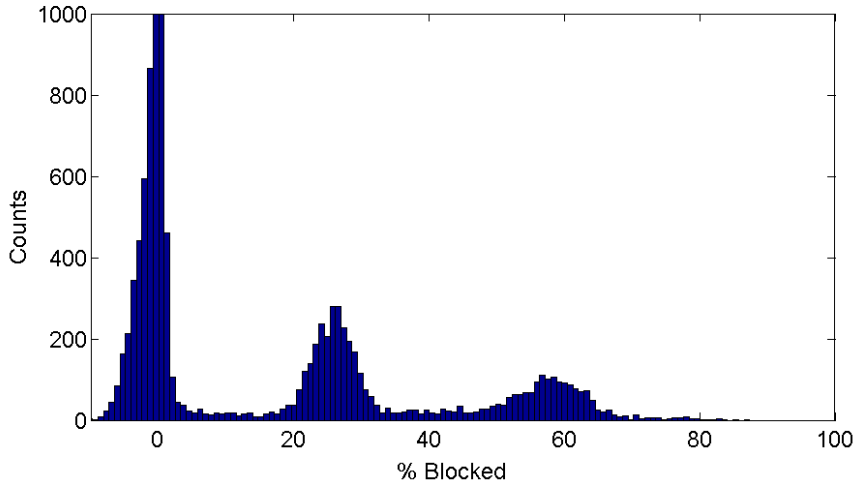

The series of all-points histograms shown above shows the influence of the selection of translocations times on the data. Once we reach a translocation time range that represents the range when most events occur, we see two well-defined peaks which correspond with the two peaks shown in the single-point-per-event histogram. The all-points histograms provide a more accurate estimate of the most common % blocked because it includes all points in the event, rather than just the lowest point. In this example, the two peaks that emerge are: 1) the main translocation peak at ~ 58 % blocked and 2) the peak indicating the shallow level at ~ 26 % blocked. In this dataset, there are actually more points at the shallow level than the deep level, but as indicated in the single-point-per-event histogram, most events contain the deep level, and there are very few events with the shallow level alone. Complete results from each type of analysis are given in the Supporting Table ST-1 for all nanopores analyzed in this work. Cited ΔG values, however, correspond to the all-points analysis.

SI-5: Molecular dynamics system setup and test of employed potential

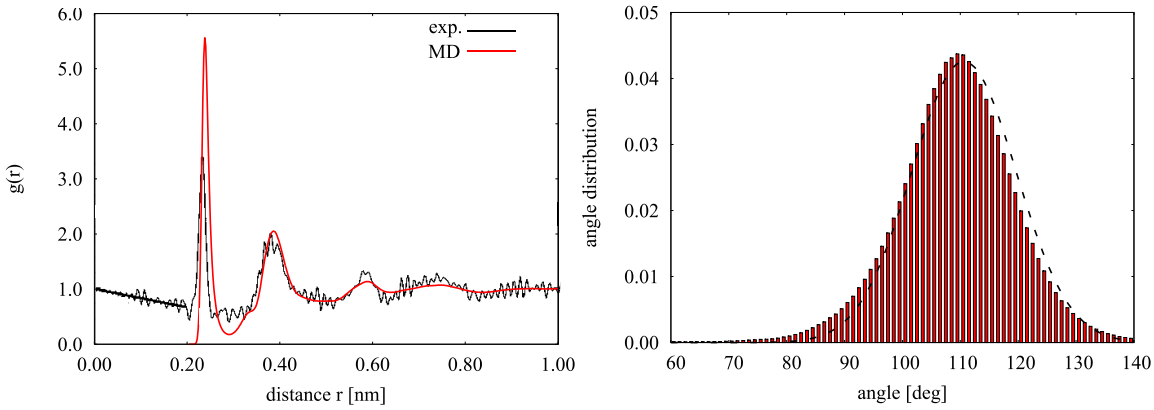

As explained in the Materials and Methods section, we employed the method of "melting and quenching" to generate initial spatial coordinates of *a*-Si bulk material. The amorphous structure was obtained by, first, equilibrating a crystalline system at a high temperature of T =3500 K during 100 ps and then quenching it to T = 500 K during 3 ns. Then, the structural properties of the corresponding *a*-Si bulk material were compared with experimental data. Here we show (left panel Figure) that there is good agreement between the theoretical estimated radial distribution function[6] (RDF) and experiment.[7] The experimental RDF was extracted from Figure 12 in reference (7). The angular distribution of the bonds between first neighbors is shown in the right panel Figure. The mean angle of the distribution is equal to 109.6° with a standard deviation of 9.5°, in good agreement with the work of Djordević *et al.*[8] and Krzeminski *et al.*[9]

SI-6: TEM images of the same STEM-thinned nanopore before and after piranha treatment and exposure to air for about one week.

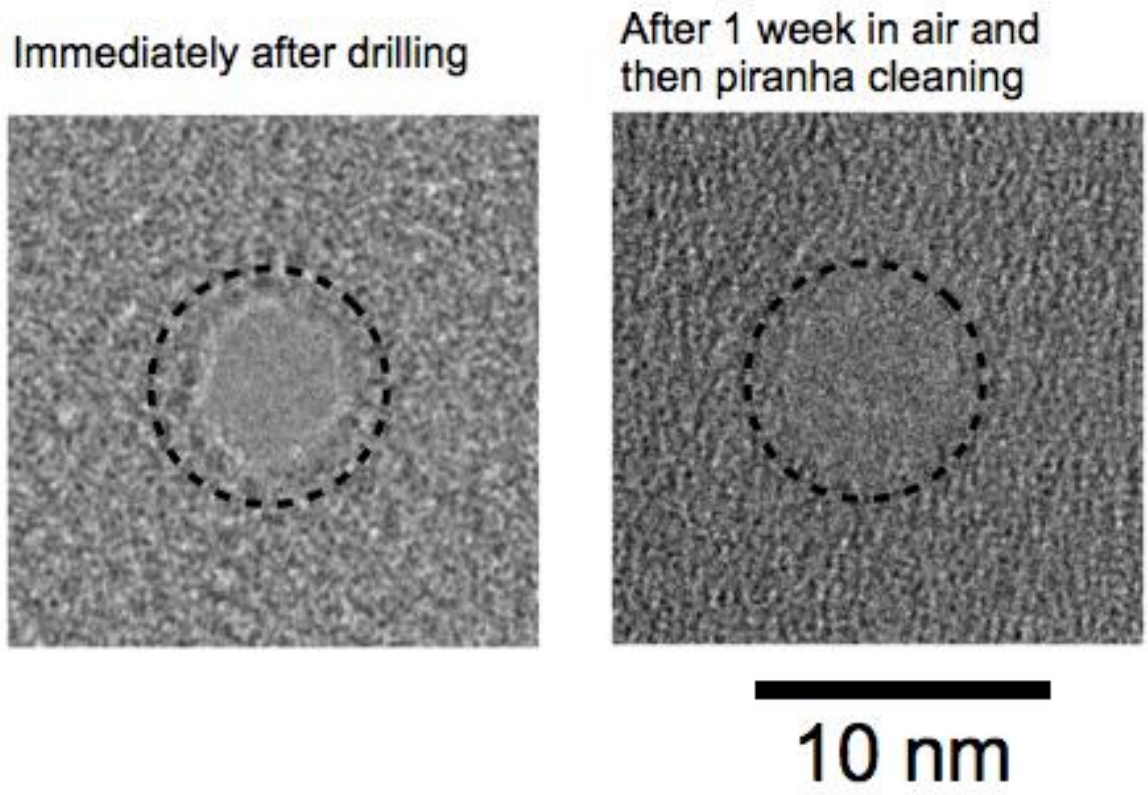

TEM images of the same STEM-drilled nanopore immediately after drilling in vacuum, and then after piranha treatment and air exposure for about one week. The two circles have identical radii in both images.

ST-1: Complete datasets for all nanopores

			All-points histogram analysis, filtered				Lowest point per event analysis				Nanopore dimensions				Error		Scaling		
Nanopore	# of events (@ 500 mV)	G_0 (nS)	% Blocked (ΔG / G_0) x 100	ΔG (nS)	Shallow level % blocked	Shallow level ΔG_s (nS)	% Blocked (ΔG / G_0) x 100	ΔG (nS)	Shallow level % blocked	Shallow level ΔG_s (nS)	Nanopore diameter TEM (nm)	Nanopore diameter fitted (nm)	Film thickness EELS (nm)	Film thickness fitted (nm)	Error in G_0 (nS) (RMS noise from 1s of data @ 500 mV)	Error in ΔG (nS) (stan. dev. from histogram)	KCl conductivity (S m^{-1})	Scaled G_0 (nS)	Scaled ΔG (nS)
S1	744	8.9	85.2	7.6	—	—	92.8	8.3	—	—	4.1	2.3	—	4.0	0.04	0.2	12.16	7.9	6.8
S2 — folding	712	23.4	22.4 and 69	5.2	—	—	38.3 and 79	9.0	—	—	5.3	4.2	—	3.9	0.1	0.6	12.16	20.8	4.7
S3	139	11.6	72.3	8.4	55.6	6.4	79.8	9.3	—	—	3.1	2.5	—	3.1	0.2	0.2	12.16	10.3	7.4
S4	870	6.6	58.4	3.9	—	—	65.5	4.3	—	—	3.2	2.8	—	9.1	0.2	0.1	12.16	5.9	3.4
S5	1835	14.0	63.9	8.9	30.0	4.2	71.4	10.0	38.2	5.3	4.0	2.6	—	2.6	0.2	0.2	12.16	12.4	7.9
S6	182	5.8	69.4	4.0	54.6	3.2	89.4	5.2	—	—	3.3	2.6	—	9.1	0.1	0.1	12.16	5.1	3.6
S7	3044	21.0	35.3	7.4	19.1	4.0	41.6	8.7	24.0	5.0	4.7	3.4	—	2.5	0.3	0.4	12.16	18.7	6.6
S8	1312	29.1	25.1	7.3	10.8	3.1	29.1	8.5	14.0	4.1	2.5	3.8	—	1.7	0.4	0.4	12.16	25.8	6.5
S9	1408	10.1	80.8	8.2	42.9	4.3	95.0	9.6	66.5	6.7	2.5	2.4	—	3.5	0.1	0.2	12.16	9.0	7.3
S10	443	18.7	57.7	10.8	25.9	4.8	62.5	11.7	31.6	5.9	—	2.7	1.5	1.5	0.2	0.4	12.0	16.8	9.7
S11	493	14.5	73.1	10.6	42.4	6.2	82.6	12.0	55.1	8.0	2.6	2.5	1.5	2.0	0.1	0.2	12.2	12.8	9.4
S12	3911	24.9	41.2	10.2	16.7	4.1	43.8	10.9	19.9	4.9	4.6	3.0	1.4	1.1	0.2	0.4	12.2	22.0	9.1

REFERENCES

(1) Kowalczyk, S. W.; Grosberg, A. Y.; Rabin, Y.; Dekker, C. Modeling the Conductance and DNA Blockade of Solid-State Nanopores. *Nanotechnol.* **2011,** *22*, 315101.

(2) Wanunu, M.; Dadosh, T.; Ray, V.; Jin, J.; McReynolds, L.; Drndić, M. Rapid Electronic Detection of Probe-Specific MicroRNAs Using Thin Nanopore Sensors. *Nat. Nanotechnol.* **2010,** *5*, 807.

(3) Carlsen, A. T.; Zahid, O. K.; Ruzicka, J.; Taylor, E. W.; Hall, A. R. Interpreting the Conductance Blockades of DNA Translocations through Solid-State Nanopores. *ACS Nano* **2014,** *8*, 4754-4760.

(4) Garaj, S.; Liu, S.; Golovchenko, J. A.; Branton, D. Molecule-Hugging Graphene Nanopores. *Proc. Natl. Acad. Sci. U. S. A.* **2013,** *110*, 12192-12196.

(5) *CRC Handbook of Chemistry and Physics,*79th ed.; Lide, D. R., Ed.; CRC Press: Boca Raton, 1998.

(6) Stillinger, F. H.; Weber, T. A. Computer Simulation of Local Order in Condensed Phases of Silicon. *Phys. Rev. B* **1985,** *31*, 5262-5271.

(7) Laaziri, K.; Kycia, S.; Roorda, S.; Chicoine, M.; Robertson, J. L.; Wang, J.; Moss, S. C. High-Energy X-ray Diffraction Study Of Pure Amorphous Silicon. *Phys. Rev. B* **1999**, 60, 13520-13533.

(8) Djordjević, B. R.; Thorpe, M. F.; Wooten, F. Computer Model of Tetrahedral Amorphous Diamond. *Phys. Rev. B* **1995,** *52*, 5685-5689.

(9) Krzeminski, C.; Brulin, Q.; Cuny, V.; Lecat, E.; Lampin, E.; Cleri, F. Molecular Dynamics Simulation of the Recrystallization of Amorphous Si layers: Comprehensive Study of the Dependence of the Recrystallization Velocity on the Interatomic Potential. *J. Appl. Phys.* **2007,** *101*, 123506.